J Mater Sci (2016) 51:1400–1408
DOI 10.1007/s10853-015-9459-1

Effect of pre-thermal treatment on the lithium storage performance of $LiNi_{0.8}Co_{0.15}Al_{0.05}O_2$

Zewen Ruan[1] · Yongming Zhu[1] · Xiangguo Teng[1]

Received: 22 July 2015 / Accepted: 22 September 2015 / Published online: 29 September 2015

Abstract Layered $LiNi_{0.8}Co_{0.15}Al_{0.05}O_2$ cathode materials have been synthesized by co-precipitation methods. The effect of pre-thermal treatment was investigated by thermogravimetric differential thermal analysis. Although X-ray diffraction has confirmed that all diffraction peaks in XRD patterns for samples treated at 500 ~ 750 °C can be a well-indexed hexagonal structure, the status of nickel ions varied. Samples pre-treated at different temperatures show different colors and had various contents of Ni^{3+} measured by XPS. Powders that heated again at 800 °C under the condition of dried oxygen for 12 h after pre-thermal treatment show different electrochemical performances, which pre-thermal treated at 600 °C had a highest reversible specific capacity about 180 $mAh \cdot g^{-1}$ and capacity retention of 91.7 % after 50 cycles when cycled at a current density of 0.1 C between 2.5–4.3 V at room temperature. The relationship between the status of nickel ions and electrochemical performance was discussed. On the other hand, the capacity retention rates are 91.7, 96.6, and 98.0 % after 50 cycles at 0.1 C and at 100 %DOD, 80 DOD, and 50 %DOD.

Introduction

$LiNiO_2$ is considered as a very promising positive electrode material for lithium-ion batteries due to its high specific capacity up to 180 ~ 220 $mAh \cdot g^{-1}$. Nevertheless, it has some shortcomings: difficulties in preparation, capacity fading during cycling, thermal instability in its charged state, and mixing of Li^+ and Ni^{2+} due to their similar size (i.e., 0.76 Å for Li^+ vs. 0.69 Å for Ni^{2+}) [1–7]. In order to overcome these disadvantages, several partial substitutions for nickel have been investigated: Al [8–10], Co [11–13], Mn [14–16], Mg [17, 18], Ti [19, 20], Fe [17], and Ga [21]. Partial substitution has shown a positive effect on the thermal stabilization of the $LiNiO_2$ in its charged state, and in all of them, cobalt partial substitution shows the best performance [11–13]. Ohzuku [22] studied the cathode materials $LiNi_xCo_{1-x}O_2$ with different proportions of nickel and cobalt, suggested that $LiNi_xCo_{1-x}O_2$ is a solid solution of $LiCoO_2$ and $LiNiO_2$. In previous reports on the $LiNi_{1-y}Al_yO_2$ system [8–10], it was found that partial aluminum substitution can further improve the thermal stabilization of $LiNiO_2$ due to the stability of the Al^{3+} ions in tetrahedral sites with stronger Al–O bond than Ni–O bond and Co–O bond [23]. Co- and Al-doped $LiNi_{1-x-y}Co_xAl_yO_2$ system has attracted more and more attentions due to its high reversible capacity and excellent cycling performance.

Recently, $LiNi_{1-x-y}Co_xAl_yO_2$ powders were synthesized by various methods. Among them, the co-precipitation is well known as one of the most suitable methods for industrial production. During the preparation processes, nickel ions of the precursors always exist in the form of Ni^{2+}. They are hard to be oxidized to Ni^{3+} ions completely even under pure oxygen, due to Ni^{2+} ions are more stable than Ni^{3+} ions at high temperature [24, 25], which leads to the mixing of Li^+ ions in the 3 a (000) positions and Ni^{2+} ions in the 3 b (001/2) positions [1, 3]. Furthermore, metal ions mixing in cathode materials deteriorate the crystal structure and electrochemical performance [1]. Changes in the surface structure of $LiNi_{0.8}Co_{0.15}Al_{0.05}O_2$

✉ Yongming Zhu
hitonline@163.com

[1] Department of Applied Chemistry, Harbin Institute of Technology at Weihai, Wenhua West Road 2#, Weihai 264209, Shandong Province, China

cathode materials were investigated by Hwang [26], Bak [27], and Watanabe [28]. They found not only the surface changes from the layered structure (space group *R*-3m) to the disordered spinel structure (*Fd*-3 m) and eventually to the rock-salt structure (*Fm*-3m) in the extent of first charge, but also a NiO-like resistance layer with *Fm*-3m rock-salt structure was formed on each primary particle during cycling tests, which result in the capacity fading of $LiNi_{0.8}Co_{0.15}Al_{0.05}O_2$. According to facts mentioned above, it is necessary to decrease the formation of Ni^{2+} ions during synthesis processes.

In this paper, layered $LiNi_{0.8}Co_{0.15}Al_{0.05}O_2$ cathode materials are synthesized by co-precipitation method, structural and electrochemical properties of $LiNi_{0.8}Co_{0.15}Al_{0.05}O_2$ are also investigated. The effect of pre-thermal treatment on the material properties was studied, especially; the crystal structure and the amounts of Ni^{2+} and Ni^{3+} ions in samples after pre-treatment were determined by XRD and XPS analysis, which will affect the electrochemistry properties of the resulting material directly. The possible reasons why samples pre-treated at different temperatures show different colors and the relationship between this phenomenon and electrochemical performance were also discussed.

Experimental

The precursor of $Ni_{0.8}Co_{0.15}Al_{0.05}(OH)_{2.05}$ was synthesized by a co-precipitation method in aqueous solution. $Ni(NO_3)_2{\cdot}6H_2O$ (A.R. 98.0 %, Aladdin Co.), $Co(NO_3)_2{\cdot}6H_2O$ (A.R. 99.0 %, Aladdin Co.), $Al(NO_3)_3{\cdot}9H_2O$ (A.R. 99.0 %, Aladdin Co.), and NaOH (A.R. 96.0 %, Aladdin Co.) were used as the starting materials. An aqueous solution of $Ni_{0.8}Co_{0.15}Al_{0.05}(NO_3)_{2.05}$ with a concentration of 1.0 M was pumped into a beaker (volume 2 L) with the speed of 0.04 L/h, at the same time, 2.0 M NaOH and NH_4OH solution were also fed into the same beaker. Temperature and pH value were controlled at 50 °C and 10.5. After vigorous stirring for 12 h, the homogenous precipitated hydroxide powder of $Ni_{0.8}Co_{0.15}Al_{0.05}(OH)_{2.05}$ was filtered off, washed, and dried at 120 °C for 24 h. The resulting powders were thermal treated at 500 ~ 750 °C under air for 4 h, then $Ni_{0.8}Co_{0.15}Al_{0.05}O_y$ and $LiOH{\cdot}H_2O$ were added together, and ball-milled with the molar ratio of (Li/(Ni + Co + Al) = 1.05). An excess of lithium was used to compensate for lithium loss during the calcinations. After grinding with lithium source, the products were heated again at 800 °C under dry oxygen for 12 h. The processes of synthesis are shown in Fig. 1.

The crystalline structure of the samples were characterized by using a D/max 2500 X-ray diffractometer, which was equipped with a diffracted-beam monochromator (Cu $K\alpha$ radiation) in the range of 10°–90°(2θ) using 0.02°(2θ) steps of a 2 s duration for routine characterization. XPS measurement was performed to examine the oxidation state of nickel ions by recording on ESCA-LAB MKII apparatus with a monochromatic Al $K\alpha$ X-ray source. During XPS measurements, the base pressure of sample chamber was kept below 3.0×10^{-10} Mbar. Emission lines were calibrated with C 1 s signal at 284.6 eV. In addition, the amount of Ni^{3+} in the samples is calculated by the peak area ratio of $Ni^{3+}/(Ni^{2+}+Ni^{3+})$. The thermogravimetric–differential thermal analysis was performed on DTG-60 H (TA Instruments, Japan) with a heating rate of 10 °C/min^{-1} under air atmosphere from room temperature to 900 °C.

The electrochemical performances of $LiNi_{0.8}Co_{0.15}Al_{0.05}O_2$ were investigated using a CR2025 coin-type cell, which were carried out in Li//1 M $LiPF_6$ in a mixture of ethylene carbonate (EC), diethyl carbonate (DEC), and dimethyl carbonate (DMC) (1:1:1 by volume)//$LiNi_{0.8}Co_{0.15}Al_{0.05}O_2$ system. The conductive agent was 10 wt% acetylene black, and 10 wt% polyvinylidene fluoride (PVDF) was used as binder with nmethyl pyrrolidone (NMP) as the solvent, then dried at 120 °C for 14 h in a vacuum oven. The positive electrodes of 12.5 mm diameter were punched out, and the thickness of positive film was 30 µm, which means the active material was 3.0 mg/cm^2. Cells were assembled in an argon-filled dry box and conducted on a battery test system (LAND CT 2001A, China) with galvanostatic charge/discharge in the voltage range of 2.5–4.3 V at room temperature for electrochemical properties. Cyclic voltammetry (CV) and impedance spectroscopy (EIS) were employed by electrochemical work station (CHI660a, China). CV tests were carried out in the voltage range of 3.0–4.8 V with a scan rate of 0.05 mV·s^{-1}, and EIS tests were carried out with the frequency ranging from 0.01 Hz to 100 kHz.

Characterization

Properties of $Ni_{0.8}Co_{0.15}Al_{0.05}(OH)_{2.05}$

Figure 2 presents the TG/DTA curves of thermal decomposition of $Ni_{0.8}Co_{0.15}Al_{0.05}(OH)_{2.05}$. The TG curve displays that weight loss takes place in the following four steps. Firstly, 6.73 % weight loss between 30 and 230 °C is ascribed to the removal of adsorbed water in the precursor powders and crystallization water Eq. (1); in the second step, a well-defined weight loss in the range of 230–400 °C can be ascribed to the decomposition of $Ni_{0.8}Co_{0.15}Al_{0.05}(OH)_{2.05}$ and transform into $Ni_{0.8}Co_{0.15}Al_{0.05}O_{1.025}$ with 19.14 % weight loss Eq. (2). The DTA curve shows one endothermic peak at 307.19 °C corresponding to the hydroxide decompose sharply. As the temperature

Fig. 1 Synthesis process of $LiNi_{0.8}Co_{0.15}Al_{0.05}O_2$ materials

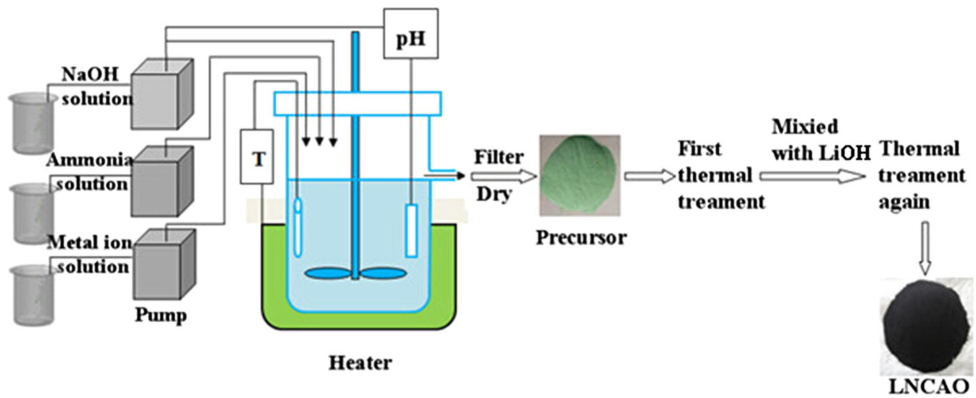

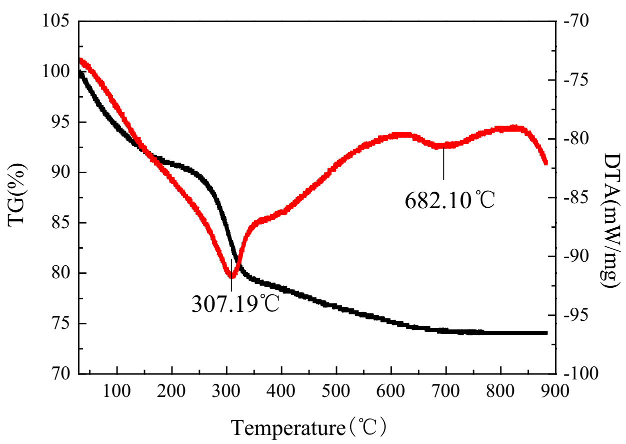

Fig. 2 TG/DTA curves of $Ni_{0.8}Co_{0.15}Al_{0.05}(OH)_{2.05}$ in air with a heating rate of 10 °C·min^{-1}

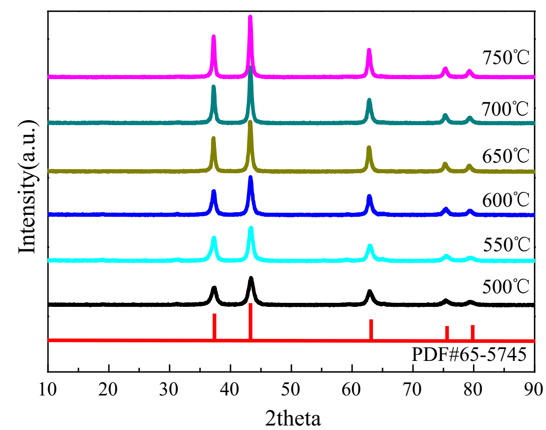

Fig. 3 XRD patterns of $Ni_{0.8}Co_{0.15}Al_{0.05}O_y$ obtained after the first thermal treatment

increases above 400 °C, partly Ni^{2+} ions were oxidized to Ni^{3+} ions Eq. (3). The fourth step of weight loss between 600 and 750 °C is attributed to the reduction of Ni^{3+} ion, because of the higher stability of Ni^{2+} ions at elevated temperature [24, 25], and it is evidenced by an obvious endothermic peak at 682.10 °C in DTA curve Eq. (4). Finally, the chemical active oxide of $Ni_{0.8}Co_{0.15}Al_{0.05}O_y$ is obtained. It is a remarkable fact that the chemical performance of Ni^{2+} obtained at different temperatures varies.

$$Ni_{0.8}Co_{0.15}Al_{0.05}(OH)_{2.05}\cdot xH_2O \rightarrow Ni_{0.8}Co_{0.15}Al_{0.05}(OH)_{2.05} \quad (1)$$

$$Ni_{0.8}Co_{0.15}Al_{0.05}(OH)_{2.05} \rightarrow Ni_{0.8}Co_{0.15}Al_{0.05}O_{1.025} \quad (2)$$

$$Ni_{0.8}Co_{0.15}Al_{0.05}O_{1.025} \rightarrow \overset{+2}{\underset{0.8-\alpha}{Ni}}\,\overset{+3}{\underset{\alpha}{Ni}}\,Co_{0.15}Al_{0.05}O_x \quad (3)$$

$$\overset{+2}{\underset{0.8-\alpha}{Ni}}\,\overset{+3}{\underset{\alpha}{Ni}}\,Co_{0.15}Al_{0.05}O_x \rightarrow \overset{+2}{\underset{0.8-\alpha+\beta}{Ni}}\,\overset{+3}{\underset{\alpha-\beta}{Ni}}\,Co_{0.15}Al_{0.05}O_y. \quad (4)$$

XRD patterns of $Ni_{0.8}Co_{0.15}Al_{0.05}O_y$ obtained after the first thermal treatment are shown in Fig. 3. All diffraction peaks for six samples can be well indexed in a NiO hexagonal structure, which belongs to cubic system with *Fm*-3m space group. As the temperature increases from 500 to 750 °C, all the peaks in the patterns become sharper and stronger, indicating the improved crystallinity of the materials. Due to different ion status in metal oxide, the metal oxide with different colors were obtained, which change from black to yellowish brown (Fig. 4). The reason of this result may be attributed to the reduction of Ni^{3+} ion. In order to get the further reason, XPS was used to examine the valence states of nickel ions of samples. Figure 5a$_1$–f$_1$ shows Ni 2p XPS data for samples treated at 500, 550, 600, 650, 700, and 750 °C, respectively. With increasing the treatment temperature

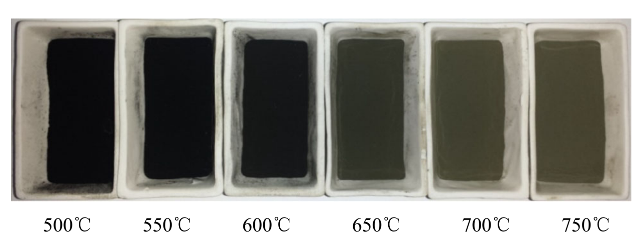

Fig. 4 Pictures of six samples after the first thermal treatment at various temperature

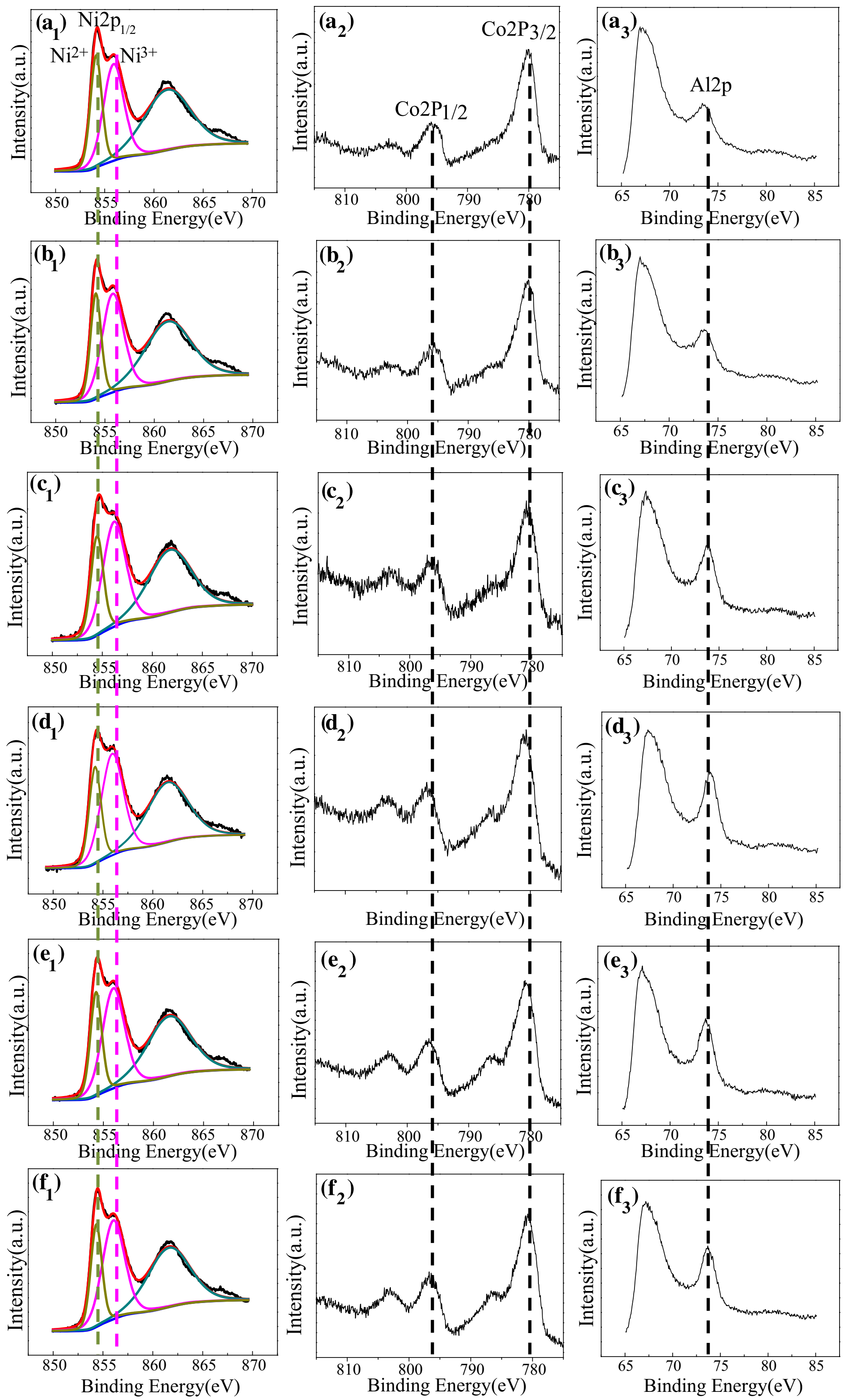

Fig. 5 XPS data of Ni 2p, Co 2p, Al 2p for samples after the first thermal treatment at various temperatures: **a** 500 °C **b** 550 °C **c** 600 °C **d** 650 °C **e** 700 °C **f** 750 °C

from 500 to 600 °C, the most intense peaks corresponding to Ni $2p_{1/2}$ shifted from lower binding energy of 855.88–855.93 eV but decreased to 885.83 eV when treatment temperature continuously increased to 750 °C, suggesting that the amount of Ni^{3+} in six samples progressively increased and then decreased [29–31]. Furthermore, when using mixed Gaussian–Lorentzian profiles, as shown in Table 1, Ni $2p_{3/2}$ peaks are well fitted in two sub-signals at 854.18–854.73 eV for Ni^{2+} with FWHM of 1.370–1.411 eV, and 855.83–855.93 eV for Ni^{3+} with FWHM of 2.436–3.727 eV, respectively. According to the fitting results, the relative content of Ni^{3+} in the six samples varies from 63.83 to 65.90 %, which is calculated by the peak area ratio of $Ni^{3+}/(Ni^{2+}+Ni^{3+})$. Figure 5a$_2$–f$_2$ shows the XPS spectra of Co 2p core level. The most intense peak at 780 eV is due to the Co $2p_{3/2}$ main peak, and the peak at 796 eV is assigned to the Co $2p_{1/2}$ main peak, which on behalf of the two spin–orbits splitting peaks. The other two weak peaks were corresponding to satellite peaks. Finally, core level of Al 2p is shown in Fig. 5a$_3$–f$_3$ indicating the precipitation of Al^{3+} ions.

Properties of $LiNi_{0.8}Co_{0.15}Al_{0.05}O_2$

It is well known that because of the similar ionic size, a disordered arrangement between transition Li layer (3b site) and metal layer (3a site) is possible, as shown in Fig. 6. Much more existing Ni^{2+} ions could not be oxidized to Ni^{3+} when the materials were treated at high temperature due to the higher stability of Ni^{2+} [24, 25]. Replacing the position of Li^+ ions would block the intercalation and de-intercalation process and induce less amount of Li^+ ions in 3b site, which leads to a decrease in reversible capacity. Furthermore, the decrease thickness of LiO_6 octahedron layer results from Ni^{2+} with smaller radius occupies at Li layer, which does not favor the processes of lithium ion's intercalation and de-intercalation. This will lead to the deterioration of electrochemical performance [24, 32]. At the same time, the increasing thickness of MO_6 octahedron layer resulting from Li^+ with largest radius in transition metal layer will weak the bond strength, which declines the thermal stability of $LiNi_{0.8}Co_{0.15}Al_{0.05}O_2$ [6, 7, 31, 33].

XRD pattern of prepared $LiNi_{0.8}Co_{0.15}Al_{0.05}O_2$ (first thermal treated at 600 °C for 4 h and treated again at 800 °C for 12 h) is shown in Fig. 7. It demonstrates that the diffraction peaks of the $LiNi_{0.8}Co_{0.15}Al_{0.05}O_2$ match well with $LiNiO_2$ phase, indexed in a rhombohedral structure of α-$NaFeO_2$ type, which belongs to *R*-3m space group [32, 34]. The I(003)/I(104) intensity ratio is about 1.65 for as-prepared $LiNi_{0.8}Co_{0.15}Al_{0.05}O_2$ under dry oxygen atmosphere. The ratio is higher than 1.2 (= 1.65) which

Table 1 XPS data of Ni 2p for samples after the first thermal treatment at various temperatures

Samples (°C)	Ni^{2+}		Ni^{3+}		$Ni^{3+}/(Ni^{2+}+Ni^{3+})$ (%)
	Peak (eV)	FWHM (eV)	Peak (eV)	FWHM (eV)	
500	854.18	1.381	855.83	2.437	63.83
550	854.18	1.396	855.88	2.576	64.85
600	854.48	1.411	855.88	2.727	65.90
650	854.73	1.404	855.93	2.636	65.25
700	854.43	1.393	855.88	2.576	64.90
750	854.43	1.370	855.83	2.436	64.00

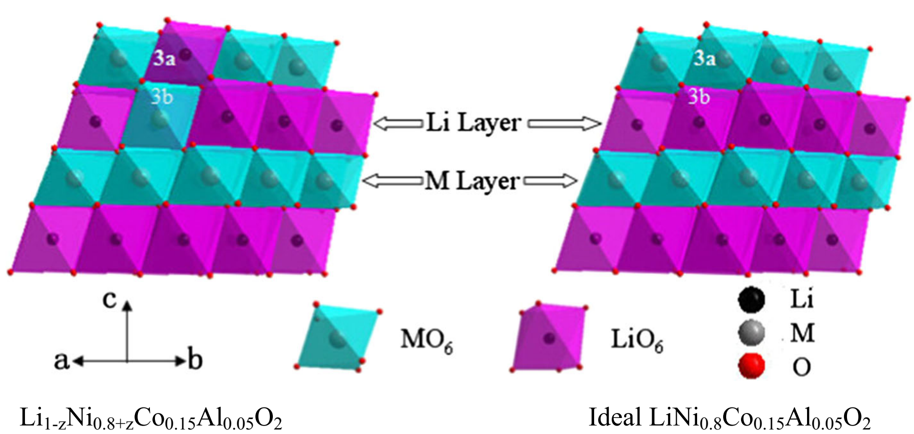

Fig. 6 Crystal structure of $Li_{1-z}Ni_{0.8+z}Co_{0.15}Al_{0.05}O_2$ and ideal $LiNi_{0.8}Co_{0.15}Al_{0.05}O_2$

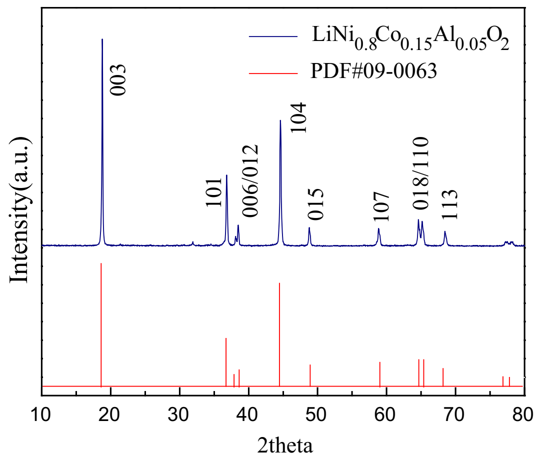

Fig. 7 XRD pattern of $LiNi_{0.8}Co_{0.15}Al_{0.05}O_2$ powers

indicates the mixing of Li^{+} ions and Ni^{2+} ions between the slab and the interslab space suppressed [1–4, 32], which shows better electrochemical performance.

Electrochemical study

Figure 8a compares the first charge and discharge capacity of cell at 0.1 C rate in the range of 2.5–4.3 V after the first thermal treatment at different temperatures. A highest reversible capacity about 180 mAh·g^{-1} is obtained for $LiNi_{0.8}Co_{0.15}Al_{0.05}O_2$, which suggests that the material heated at 600 °C shows the best electrochemical performance. Figure 8b presents cycle performance of pre-treated $LiNi_{0.8}Co_{0.15}Al_{0.05}O_2$ at a current density of 0.1 C between 2.5 and 4.3 V. The capacity of sample pre-treated at 600 °C only decreased from 181 to 166 mAh/g at the rate of 0.1 C under room temperature after 50 cycles and showed good cycle performance (Fig. 8c) and 91.7 % capacity retention (Table 2). Figure 8c compares the rate performances of the cells evaluated at variable current rates of 0.1–2 C for 5 cycles, it is clearly discerned that the capacities of all cells decreased as cycling current rate increased, due to the low diffusion rate of the Li^{+} ions intercalate/de-intercalate electrodes at high rate [35]. To further prove the cycle performance of $LiNi_{0.8}Co_{0.15}Al_{0.05}O_2$ pre-treated at 600 °C, the discharge at different depth was investigated in Fig. 8d. The capacity retention of cells at 100 %DOD, 80, and 50 %DOD were 91.7, 96.6, and 98.0 % after 50 cycles at 0.1 C, respectively. It may imply that the $LiNi_{0.8}Co_{0.15}Al_{0.05}O_2$ positive electrode has good electrochemical reversibility and structural stability.

On one hand, poorly crystalline material usually has more defects, which means a large number of carriers, and the improvement of crystallinity is often accompanied by the increase of particle size and decrease of specific surface area.

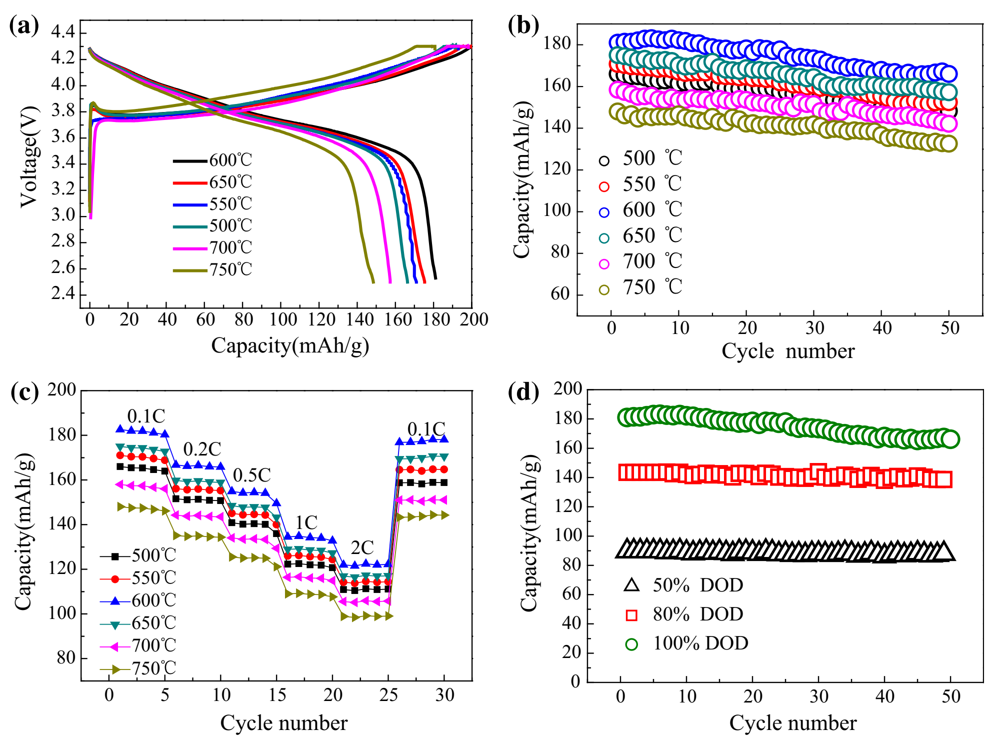

Fig. 8 Electrochemical performance tests: **a** Initial charge and discharge curves of the $LiNi_{0.8}Co_{0.15}Al_{0.05}O_2$ at 0.1 C. **b** Cycle performance of the $LiNi_{0.8}Co_{0.15}Al_{0.05}O_2$at 0.1 C. **c** Rate capability under variable current rate of the $LiNi_{0.8}Co_{0.15}Al_{0.05}O_2$. **d** Cycle performance under various depth of discharge (DOD) of the $LiNi_{0.8}Co_{0.15}Al_{0.05}O_2$ pre-treated at 600 °C at 0.1 C

Table 2 Electrochemical performance of the samples

Samples (°C)	Initial charge capacity (mAh/g)	Initial discharge capacity (mAh/g)	Columbic efficiency (%)	Capacity retention after 50 cycles at 0.1 C (%)
500	191.6	166.4	86.8	89.3
550	193.0	171.1	88.7	89.2
600	206.8	181.1	87.6	91.7
650	204.0	175.3	85.9	89.9
700	190.2	157.3	82.7	89.9
750	180.7	148.5	82.2	89.6

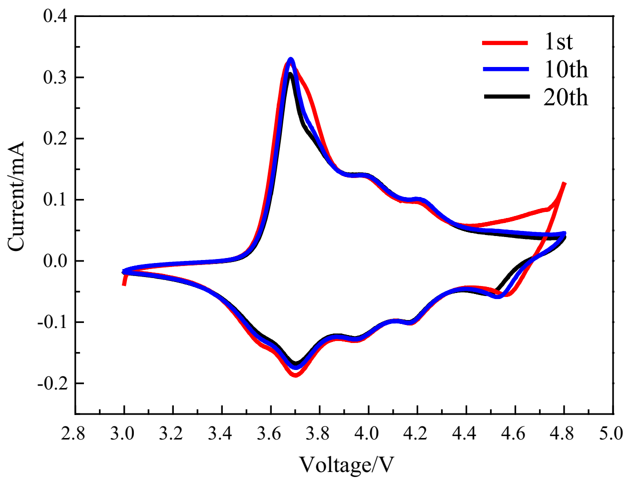

Fig. 9 CV curves of $LiNi_{0.8}Co_{0.15}Al_{0.05}O_2$ versus. Li in the voltage range of 3.0–4.8 V with a scan rate of 0.05 mV/s

On the other hand, according to TG–DTA curve and the results of XPS analysis, partial Ni^{2+} will transform into Ni^{3+} with increasing temperature to 400 ∼ 600 °C, and some of Ni^{3+} will be reduced to inactive Ni^{2+} with increasing temperature more than 600 °C. But the decomposition process of precursor is strictly not in accordance with the four steps mentioned above. In other words, the precursor not completely decomposed at 200 ∼ 400 °C may continue to decompose with increasing temperature even to 600°C and Ni^{2+} was oxidized to Ni^{3+} at the same time. The competition between oxidization of Ni^{2+} to Ni^{3+} and reduction of Ni^{3+} to Ni^{2+} with low chemical activation leads to higher content of Ni^{3+}. Compared with others, nickel ion can transform into Ni^{3+} as much as possible with less mixing of Li^{+} ions and Ni^{2+} ions in final materials.

A CV measurement is very helpful to understand the electrochemical reactions at the electrode of the cell during the charging and discharging process. Figure 9 shows CV curves of the $LiNi_{0.8}Co_{0.15}Al_{0.05}O_2$ electrode versus Li reference electrode. Peaks are observed at 3.68, 3.95, and 4.20 V with lithium extraction from the oxide. And the corresponding peaks during lithium insertion into the oxide are at 3.70, 3.95, and 4.17 V. These three couples of peaks corresponding to different phase transition processes are accompanied by the intercalation and de-intercalation of lithium ions [17, 36]. The small potential separation between the oxidation and reduction peaks of 0.03 V suggests that $LiNi_{0.8}Co_{0.15}Al_{0.05}O_2$ electrode has good

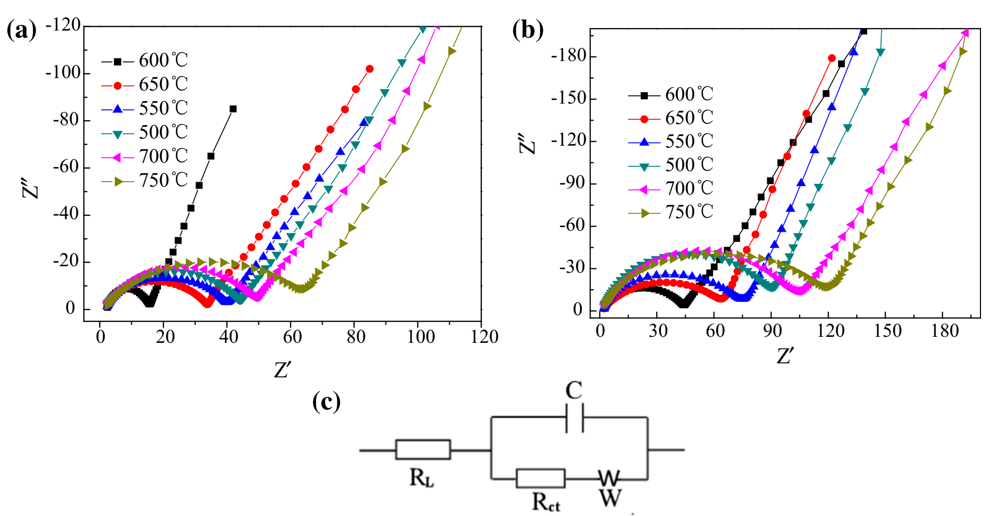

Fig. 10 Impedance spectra of $LiNi_{0.8}Co_{0.15}Al_{0.05}O_2$ vs Li: **a** after first cycle **b** after 50 cycles **c** equivalent circuit

Table 3 Independent resistive components analyzed using an equivalent circuit

Samples (°C)	After first cycle				After 50 cycles			
	R_L (Ω/cm^2)	R_{ct} (Ω/cm^2)	C (10^{-6}μF/cm^2)	W (10^{-3}S. sec^5/cm^2)	R_L (Ω/cm^2)	R_{ct} (Ω/cm^2)	C (10^{-6}μF/cm^2)	W (10^{-3}S.sec^5/cm^2)
500	2.881	32.41	8.966	4.199	3.222	61.49	0.743	1.441
550	2.567	28.76	6.341	6.297	2.602	55.83	1.357	4.143
600	2.707	12.05	2.276	12.63	2.904	32.41	0.897	4.200
650	2.764	25.33	1.298	8.712	3.024	41.40	1.323	4.065
700	2.926	35.47	8.870	3.483	3.056	77.90	0.617	2.308
750	3.324	43.40	1.423	4.366	3.262	78.34	0.725	1.400

reversibility during charging and discharging with the intercalation and de-intercalation of Li^+ ions from the crystal lattice [37]. Furthermore, a peak at 4.5 ~ 4.6 V is corresponding to the oxidation reaction of Co^{3+} [38]. In addition, the first cycle curve exhibits a broad peak at 4.7 ~ 4.8 V and can be assigned to either electrolyte oxidation [39] or initial reorganization of the transform of Ni-rich cathode material to spinel phase above 4.7 V involves two cubic/cubic two-phase reactions [40], which was accompanied by release of oxygen from the spinel lattice [41]. After 10 and 20 cycles, the oxidation and reduction peaks both have a slight shift, illustrating excellent cycling performance.

Typical electrochemical EIS plots from a $LiNi_{0.8}Co_{0.15}Al_{0.05}O_2$ electrode versus Li reference electrode are shown in Fig. 10. All spectra exhibit an arc and a straight line in the high- and low-frequency regions. As can been seen in Fig. 10a and b, the impedance spectra can be explained on the basis of an equivalent circuit with ohmic resistance (R_L) from the electrolyte, separator and electrode, charge transfer resistance (Rct), double-layer capacitance, passivation film capacitance (C), and Warburg Impedance (Zw) [37]. Figure 10c is an equivalent circuit and fitting results are shown in Table 3. The starting point of arc is invariant and demonstrates that all R_L are nearly equal, and the high-frequency arc width of cell increases with cycling, which is ascribed to the phase transform, degradation of composite electrode, and the accumulation of low conductive products (like NiO) on the surface [26–28]. As can be seen that among all of them, samples pre-treated 600 °C has the lowest value of R_{ct}, which are 12.05 Ω after first cycle and 32.41 Ω after 50 cycles. Furthermore, comparison of the value of Zw in Table 3 is striking. The decreasing of Zw was accompanied by cycling tests, which due to the phase transform in surface of cathode materials (layered structure to spinel structure, even to rock-salt structure) leading to the diffusion of lithium ions became more and more difficult [26–28]. And samples pre-treated 600 °C had the highest value of Zw, which consequently shows good electrochemical performance.

Conclusion

In this work, $Ni_{0.8}Co_{0.15}Al_{0.05}(OH)_{2.05}$ precursors were prepared by co-precipitation methods, then the cathode materials with high initial capacity were synthesized after two-stage thermal treatment. The influence of first thermal treatment on materials has been investigated. With the increasing of treatment temperature, partial nickel ions were oxidized to Ni^{3+} ions and then some of Ni^{3+} ions were reduced to Ni^{2+} ions which has lower electrochemical activity with colors of metal oxide changed from black to yellowish brown. Electrochemical tests have shown $LiNi_{0.8}Co_{0.15}Al_{0.05}O_2$ electrode material treated at 600 °C has the highest reversible capacity (more than 180 mAh·g^{-1}) and excellent cycling stability, which has highest content of Ni^{3+} ions with chemical activity. We believe that this kind of cathode material may find wide application in EV, HEV, digital products, space applications, and energy storage.

Acknowledgements The financial support of Creative fund of Chinese aerospace (2014-YF-0419) and China Postdoctoral Science Foundation (2012M520717) are gratefully acknowledged.

References

1. Choi YM, Pyun SI, Moon SI, Hyung YE (1998) A study of the electrochemical lithium intercalation behavior of porous $LiNiO_2$ electrodes prepared by solid-state reaction and sol–gel methods. J Power Sources 72:83–90
2. Morales J, Vicente CP, Tirado JL (1990) Cation distribution and chemical deintercalation of $Li_{1-x}Ni_{1+x}O_2$. Mater Res Bull 25:623–630
3. Rougier A, Gravereau P, Delmas C (1996) Optimization of the composition of the $Li_{1-z}Ni_{1+z}O_2$ electrode materials: structural, magnetic, and electrochemical studies. J Electrochemical Soc 143:1168–1175
4. Dahn JR, Sacken UV, Michal CA (1990) Structure and electrochemistry of $Li_{1\pm y}NiO_2$ and a new Li_2NiO_2 phase with the $Ni(OH)_2$ structure. Solid State Ionics 44:87–97
5. Kalaiselvi N, Raajaraajan AV, Sivagaminathan B, Renganathan NG, Muniyandi N, Ragavan M (2003) Synthesis of optimized $LiNiO_2$ for Lithium ion batteries. Ionics 9:382–387

6. Lee KK, Yoon WS, Kim KB, Lee KY, Hong ST (2001) Thermal behavior and decomposition mechanism of electrochemically delithiated $Li_{1-x}NiO_2$. J Power Sources 97–98:321–325
7. Arai H, Okada S, Sakurai Y, Yamaki JI (1998) Thermal behavior of $Li_{1-y}NiO_2$ and the decomposition mechanism. Solid State Ionics 109:295–302
8. Stoyanova R, Zhecheva E, Kuzmanova E, Alcantara R, Lavela P, Tirado JL (2000) Aluminium coordination in $LiNi_{1-y}Al_yO_2$ solid solutions. Solid State Ionics 128:1–10
9. Zhong QM, Sacken UV (1995) Crystal structures and electrochemical properties of $LiAl_yNi_{1-y}O_2$ solid solution. J Power Sources 54:221–223
10. Wang GX, Zhong S, Bradhurst DH, Dou SX, Liu HK (1999) $LiAl_\delta Ni_{1-\delta}O_2$ solid solutions as cathodic materials for rechargeable lithium batteries. Solid State Ionics 116:271–277
11. Rougier A, Saadoune I, Gravereau P, Willmannb P, Delmas C (1996) Effect of cobalt substitution on cationic distribution in $LiNi_{1-y}Co_yO_2$ electrode materials. Solid State Ionics 90:83–90
12. Chen H, Dawson JA, Harding JH (2014) Effects of cationic substitution on structural defects in layered cathode materials $LiNiO_2$. J Mater Chem A 2:7988–7996
13. Mukai K, Sugiyama J, Ikedo Y, Brewer JH, Ansaldo EJ, Morris GD, Ariyoshi K, Ohzuku T (2007) Microscopic magnetism in lithium insertion materials of $LiNi_{1-x}Co_xO_2$(x = 0, 1/4, 1/2, 3/4, and 1). J Power Sources 174:843–846
14. Sekizawa O, Hasegawa T, Kitamura N, Idemoto Y (2011) Crystal and electronic structure change determined by various method for delithiation process of Lix(Ni, Mn)O2-based cathode material. J Power Sources 196:6651–6656
15. Pasero D, Reeves N, Gillie LJ, West AR (2007) Variable oxygen stoichiometry in layered rock salt cathodes, Lix(Mn, Ni)O2, depending on synthesis conditions. J Power Sources 174: 1078–1081
16. Makimura Y, Ohzuku T (2003) Lithium insertion material of $LiNi_{1/2}Mn_{1/2}O_2$ for advanced lithium-ion batteries. J Power Sources 119–121:156–160
17. Delmas C, MeÂneÂtrier M, Croguennec L, Saadoune I, Rougier A, Pouillerie C, Prado G, GruÈne M, FourneÁs L (1999) An overview of the Li(Ni, M)O2 systems: syntheses, structures and properties. Electrochimica Acta 45:243–253
18. Julien C, Nazri GA, Rougier A (2000) Electrochemical performances of layered $LiM_{1-y}M_{1-y}'O_2$ (M = Ni, Co; M′ = Mg, Al, B) oxides in lithium batteries. Solid State Ionics 135:121–130
19. Joeng JW, Kang SG (2003) Structural and electrochemical properties of $LiNi_yTi_{1-y}O_2$ prepared by a wet process. J Power Sources 123:75–78
20. Zhang LQ, Noguchi H, Li DC, Muta T, Wang XQ, Yoshioa M, Taniguchi I (2008) Synthesis and electrochemistry of cubic rocksalt Li-Ni-Ti-O compounds in the phase diagram of $LiNiO_2$-$LiTiO_2$-$Li[Li_{1/3}Ti_{2/3}]O_2$. J Power Sources 185:534–541
21. Nishida Y, Nakane K, Satoh T (1997) Synthesis and properties of gallium-doped $LiNiO_2$ as the cathode material for lithium secondary batteries. J Power Sources 68:561–564
22. Koyama Y, Makimura Y, Tanaka I, Adachi H, Ohzuku T (2004) Systematic research on insertion materials based on superlattice models in a phase triangle of $LiCoO_2$-$LiNiO_2$-$LiMnO_2$. J Electrochem Soc 151(9):A1499–A1506
23. Cao H, Xia BJ, Xu NX, Zhang CF (2004) Structural and electrochemical characteristics of Co and Al co-doped lithium nickelate cathode materials for lithium-ion batteries. J Alloy Compd 376:281–286
24. Bianchi V, Bach S, Belhomme C, Farcy J, Ramos JPP, Caurant D, Baffier N, Willmann P (2001) Electrochemical investigation of the Li insertion-extraction reaction as a function of lithium deficiency in $Li_{1-x}Ni_{1+x}O_2$. Electrochimica Acta 46:999–1011
25. Bianchi V, Caurant D, Baffier N, Belhomme C, Chappel E, Chouteau G, Bach S, Ramos JPP, Sulpice A, Wilmann P (2001) Synthesis, structural characterization and magnetic properties of quasistoichiometric $LiNiO_2$. Solid State Ionics 140:1–7
26. Hwang S, Chang W, Kim SM, Su D, Kim DH, Lee JY, Chung KY, Stach AEA (2014) Investigation of changes in the surface structure of $Li_xNi_{0.8}Co_{0.15}Al_{0.05}O_2$ cathode materials induced by the initial charge. Chem Mater 26:1084–1092
27. Bak SM, Nam KW, Chang W, Yu XQ, Hu E, Hwang S, Stach EA, Kim KB, Chung KY, Yang AX (2013) Correlating structural changes and gas evolution during the thermal decomposition of charged $Li_xNi_{0.8}Co_{0.15}Al_{0.05}O_2$ cathode materials. Chem Mater 25:337–351
28. Watanabe S, Kinoshita M, Hosokawa T, Morigaki K, Nakura K (2014) Capacity fade of $LiAl_yNi_{1-x-y}Co_xO_2$ cathode for lithium-ion batteries during accelerated calendar and cycle life tests. J Power Sources 258:210–217
29. Cho Y, Cho J (2010) Significant improvement of $LiNi_{0.8}Co_{0.15}Al_{0.05}O_2$ cathodes at 60°C by SiO_2 dry coating for Li-Ion batteries. J Electrochem Soc 157(6):A625–A629
30. Bi YJ, Yang WC, Du R, Zhou JJ, Liu M, Liu Y, Wang DY (2015) Correlation of oxygen non-stoichiometry to the instabilities and electrochemical performance of $LiNi_{0.8}Co_{0.1}Mn_{0.1}O_2$ utilized in lithium ion battery. J Power Sources 283:211–218
31. Kosova NV, Devyatkina ET, Kaichev VV (2007) Optimization of Ni2 +/Ni3 + ratio in layered Li(Ni, Mn, Co)O2 cathodes for better electrochemistry. J Power Sources 174:965–969
32. Guilmard M, Pouillerie C, Croguennec L, Delmas C (2003) Structural and electrochemical properties of $LiNi_{0.70}Co_{0.15}Al_{0.15}O_2$. Solid State Ionics 160:39–50
33. Fu CC, Li GS, Luo D, Li Q, Fan JM, Li LP (2014) Nickel-rich layered microspheres cathodes: lithium/nickel disordering and electrochemical performance. ACS Appl Mater Interfaces 6:15822–15831
34. Yang HZ, Liu PX, Chen QL, Liu XW, Lu YW, Xie SF, Ni L, Wu XY, Peng MY, Chen YB, Tang YF, Chen YF (2014) Fabrication and characteristics of high-capacity $LiNi_{0.8}Co_{0.15}Al_{0.05}O_2$ with monodisperse yolk-shell spherical precursors by a facile method. RSC Advances 4:35522–35527
35. Wang ZY, Huang SS, Chen BJ, Wu H, Zhang Y (2014) Infiltrative coating of $LiNi_{0.5}Co_{0.2}Mn_{0.3}O_2$ microspheres with layer-structured $LiTiO_2$ towards superior cycling performances for Li-ion batteries. J Mater Chem A 2(47):19983–19987
36. Lee KK, Kim KB (2000) Electrochemical and structural characterization of LiNi1–yCoyO2 ($0 \leq y \leq 0.2$) positive electrodes during initial cycling. J Electrochem Soc 147(5):1709–1717
37. Koyama Y, Tanaka I, Adachi H (2003) Crystal and electronic structures of superstructural $Li_{1-x}[Co_{1/3}Ni_{1/3}Mn_{1/3}]O_2$ ($0 \leq x \leq 1$). J Power Sources 119–121:644–648
38. Abraham DP, Kawauchi S, Dees DW (2008) Modeling the impedance versus voltage characteristics of $LiNi_{0.8}Co_{0.15}Al_{0.05}O_2$. Electrochimica Acta 53:2121–2129
39. Hassoun J, Lee KS, Sun YK, Scrosati B (2011) An advanced Lithium Ion Battery based on high performance electrode materials. J Am Chem Soc 133:3139–3143
40. Arrebola BC, Caballero A, Cruz M, Hernán L, Morales J, Castellón ER (2006) Crystallinity control of a nanostructured $LiNi_{0.5}Mn_{1.5}O_4$ spinel via polymer-assisted synthesis: a method for improving its rate capability and performance in 5 V lithium batteries. Adv Funct Mater 16:1904–1912
41. Caballero A, Hernan L, Melero M, Morales J, Angulo M (2005) Oxygen lattice instability as a capacity fading mechanism for 5 V cathode materials. J Electrochem Soc 152(1):A6–A12